

Optical line width broadening mechanisms at the 10 kHz level in $\text{Eu}^{3+}:\text{Y}_2\text{O}_3$ nanoparticles

John G. Bartholomew,^{*,†} Karmel de Oliveira Lima,[†] Alban Ferrier,^{†,‡} and Philippe Goldner[†]

[†]*PSL Research University, Chimie ParisTech, CNRS, Institut de Recherche de Chimie Paris, 75005 Paris, France*

[‡]*Sorbonne Universités, UPMC Université Paris 06, 75005, Paris, France*

E-mail: john.g.bartholomew@gmail.com

Abstract

We identify the physical mechanisms responsible for the optical homogeneous broadening in $\text{Eu}^{3+}:\text{Y}_2\text{O}_3$ nanoparticles to determine whether rare-earth crystals can be miniaturized to volumes less than λ^3 whilst preserving their appeal for quantum technology hardware. By studying how the homogeneous line width depends on temperature, applied magnetic field, and measurement time scale the dominant broadening interactions for various temperature ranges above 3 K were characterized. Below 3 K the homogeneous line width is dominated by an interaction not observed in bulk crystal studies. These measurements demonstrate that broadening due to size-dependent phonon interactions is not a significant contributor to the homogeneous line width, which contrasts previous studies in rare-earth ion nanocrystals. Importantly, the results provide strong evidence that for the 400 nm diameter nanoparticles under study the minimum line width achieved (45 ± 1 kHz at 1.3 K) is not fundamentally limited. In addition, we highlight that the expected broadening caused by electric field fluctuations

arising from surface charges is comparable to the observed broadening. Under the assumption that such Stark broadening is a significant contribution to the homogeneous line width, several strategies for reducing this line width to below 10 kHz are discussed. Furthermore, it is demonstrated that the Eu^{3+} hyperfine state lifetime is sufficiently long to preserve spectral features for timescales up to 1 s. These results allow integrated rare-earth ion quantum optics to be pursued at a sub-micron scale and hence, open up directions for greater scaling of rare-earth quantum technology.

Keywords

Rare-earth ion doped nanoparticles, Narrow optical transitions, Coherent spectroscopy, Phonon interactions, Disordered materials, Surface charge fluctuations

The optical and spin transitions of rare-earth ions in crystalline hosts are among the narrowest observed in the solid state. For example, in bulk $\text{Eu}^{3+}:\text{Y}_2\text{SiO}_5$ crystals the optical transition has a line width of 122 Hz¹ and the nuclear spin transition has a broadening of 15 μHz .² Because of these narrow transitions rare-earth-ion materials are an appealing system to pursue the realization of quantum information technology. Indeed, a number of important quantum-optical protocols have already been demonstrated including quantum memories,³⁻⁵ quantum sources,⁶ frequency conversion,^{7,8} and qubit manipulation and readout.^{9,10}

Although the rare-earth-ion system is suitable for coupling photons and spins at the quantum level, thus far such properties have only been achieved in bulk crystals. Despite their proven performance, bulk crystals impose limitations on the miniaturization of rare-earth ion quantum hardware and the performance of some protocols. One example is the high spectral resolution optical detection of single rare-earth ions.^{11,12} The work in Refs. [11,12] has shown that there are several advantages to studying single praseodymium ions in micron or sub-micron crystals rather than in a bulk crystal. In particular, the collection efficiency for single emitter fluorescence can be an order of magnitude higher when sub-micron-diameter

crystals are used.¹¹ In addition, using small crystals significantly reduces the background fluorescence due to resonant ions outside of the collection focus. Rare-earth ion nanocrystals also make it possible to optically couple to ions through the use of optical microcavities with mode volumes of the order of λ^3 [13,14]. Such systems offer an opportunity to significantly increase the coupling strength between an optical cavity and the weakly allowed $4f^N \leftrightarrow 4f^N$ transitions toward the strong cooperativity regime.^{15,16}

To advance the applications of rare-earth ion research, including single-ion devices, it is necessary to create miniaturized and integrated platforms that preserve the material’s appealing properties.^{16–18} Toward this goal, there are advantages in using a bottom-up approach for creating well-dispersed sub-micron crystals. The greatest advantage of nanocrystal growth compared to top-down approaches involving crushing and grinding bulk crystals is the ability to create a large number of highly homogeneous particles without the risk of introducing additional stochastic defects or strain in the crystal lattice.¹⁹ The bottom-up approach also allows the control and tunability of the crystals’ size, morphology, and dispersion.

The aim of this paper is to study whether the optical transition line widths of rare-earth ions in nanoparticles are sufficiently narrow to establish a foundation for pursuing miniaturized quantum hardware architectures. The optical homogeneous line width Γ_h together with the rate of spectral diffusion and nuclear spin-state lifetime ultimately limit the performance of optical protocols in rare-earth ion crystals. We present a detailed spectroscopic study of 0.5% $\text{Eu}^{3+}:\text{Y}_2\text{O}_3$ nanoparticles to examine the dominant homogeneous broadening mechanisms of the optical ${}^7\text{F}_0 \leftrightarrow {}^5\text{D}_0$ transition. In doing so, the feasibility of achieving line widths less than 10 kHz in sub-micron particles is investigated. The temperature dependence of the homogeneous line width (Γ_h) between 1.3 K and 22.5 K was studied by performing hole burning and two pulse photon echoes on powdered nanoparticle samples. We also investigated the extent of time-dependent spectral diffusion through the use of three pulse photon echoes, which also probes the nuclear spin level lifetimes of the optical ground state.

Through these measurements we determine the broadening contributions of interactions

between europium ions and dynamic disorder modes, phonons, and magnetic fluctuations within the host lattice in a system possessing the narrowest optical line width for any sub-micron diameter particle. Importantly, the presented characterization shows that the total broadening of 45 ± 1 kHz at 1.3 K is not fundamentally limited by size-dependent phonon interactions, which have been proposed as the dominant mechanism in previous studies on rare-earth ion doped nanocrystals.²⁰⁻²² As an alternate mechanism, we show that the expected broadening due to electric field perturbations arising from rapidly changing configurations of surface charge is consistent with the broadening observed in the studied sample. The consequences of a significant contribution from Stark broadening are discussed including the feasibility of probing a regime where frequency shifts due to optically controlled interactions between pairs of europium ions could be resolved. We also demonstrate that the spin-state lifetime is long enough to allow optical coherent states to be mapped onto the spin population and recalled after one second, with spectral diffusion on this time scale less than 200 kHz. Given the current properties of the studied nanoparticles and the avenues for improvement identified in this paper, rare-earth nanocrystals offer significant advances for the scalability of rare-earth quantum devices.

Because of the application of rare-earth-ion doped coatings and nanoparticles for lighting, phosphor, and laser applications, many studies have probed the optical properties of these materials, including $\text{Eu}^{3+}:\text{Y}_2\text{O}_3$.²³ Although much is known about the optical transitions of europium ions in Y_2O_3 nanoparticles, very few studies have examined the homogeneous line width at the level of precision investigated in bulk crystals. There are, however, a set of studies that concentrate on the phonon-electron interactions²⁰⁻²² and interactions between electrons and two level systems (TLS)²⁴ in rare-earth-doped nanocrystals. In these works, it was evident that the dominant broadening mechanisms in nanocrystals less than 30 nm in diameter were significantly different from bulk crystals. As shown in Fig. 1, the homogeneous line width for nanoparticles can be of the order of a factor of 10^4 broader than the narrowest

line width observed in bulk crystals. This was attributed to a greatly enhanced phonon interaction with the ion electronic states because of the confinement of vibrational excitations and the resultant atomic motion.²² Because the amplitude of the atomic motion is particle size-dependent the phononic interaction varies according to a power law d^α , where d is the nanocrystal diameter, and $\alpha \approx -2.5$ was extracted for nanocrystals containing europium.²²

Fig. 1 shows the data from Refs. [22,24] and a fit to the proposed $d^{-2.5}$ power law. The model suggests that the broadening due to the size-dependent phononic interaction will be of the order of the lifetime limit for nanoparticles (≈ 200 Hz) for $d \approx 500$ nm. Fig. 1 also includes a fit to the d^{-2} power law observed in semiconductor nanocrystals,^{25,26} which gives a size limit that is larger by approximately a factor of two. If the scaling in either of these models is correct, there would exist a significant limitation on the miniaturization of rare-earth-ion crystals for use in high spectral resolution applications, such as quantum information processing. For example, in crystals containing europium, the process of shelving ions to auxiliary nuclear spin levels of the ground state through optical pumping becomes increasingly challenging for homogeneous line widths above 1 MHz.¹ Fig. 1 suggests that requiring the use of a shelving state limits the crystallite diameter to greater than 20 nm. Even narrower line widths (typically of the order of kHz) and hence, larger crystallites, are required to reversibly map optical quantum states onto spin coherences.²⁷

The renewed interest in studying rare-earth-doped nanoparticles in high spectral resolution was initially motivated by the study of coherent processes in highly scattering media.²⁹ Our subsequent study on $\text{Eu}^{3+}:\text{Y}_2\text{O}_3$ nanoparticle powders revealed that the Γ_h of 60 nm diameter crystallites prepared with a solvothermal method³⁰ fell within the range predicted by particle size-dependent phononic interactions (see Fig. 1). Although Perrot *et al.* studied the cubic Y_2O_3 phase in contrast to the previous studies of Eu_2O_3 [22] and the monoclinic phase of $\text{Eu}^{3+}:\text{Y}_2\text{O}_3$ [24], mechanisms such as interactions with host spins and two-phonon Raman (TPR) interactions should produce similar levels of broadening in all these materials. One key difference between the results of Perrot *et al.* and these previous studies was

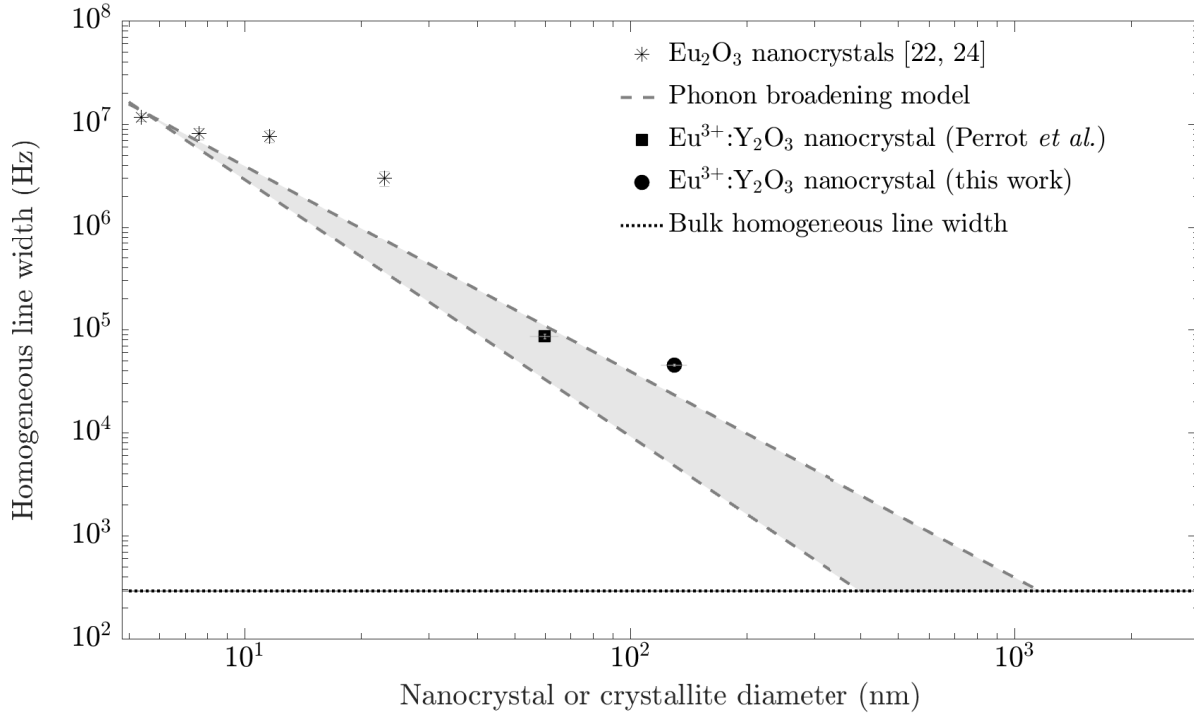


Figure 1: The relationship between nanocrystal or crystallite diameter and the homogeneous line width at 1.4 K. The shaded area representing the predictions of the phonon broadening model shows the boundary between the $d^{-2.5}$ power law proposed in Ref. [22] and the d^{-2} scaling observed in quantum dots.^{25,26} Although the data points appear consistent with the model, we show in this work that the homogeneous line width in 130 nm diameter crystallites is not dominated by size-dependent phonon interactions. This opens up opportunities for achieving bulk crystal line widths (<300 Hz²⁸) for smaller particles compared to the value suggested by the models.

the observation of a strongly linear temperature dependence of Γ_h . This is strong evidence that interactions between the electronic levels of the rare-earth ion and TLS dominate the broadening due to phonons at low temperature. In Ref. [22], TLS mediated broadening is discussed but the strong T^3 dependence of Γ_h in nanocrystals with $d = 23 \pm 3$ nm (for 1.4 K $< T < 20$ K) provided strong evidence to support particle size-dependent effects. In contrast, the conclusions of Perrot *et al.* suggest that at least one significant broadening contribution is not linked to phonon interactions. Thus, a question addressed in this work is whether rare-earth nanocrystals are a feasible candidate for quantum technology applications and what is the minimum size at which their optical properties will remain suitable.

In this work we study the interactions governing the homogeneous broadening in nanopar-

ticles comprised of single nanocrystals with $d \approx 100$ nm. Despite the measured homogeneous line width seeming consistent with the previously proposed model based on size-dependent phonon interactions, the spectroscopic analysis demonstrates that this mechanism is not limiting the observed line width. This suggests that rare-earth ion technology can be pursued on smaller scales than previously thought possible.

0.5% $\text{Eu}^{3+}:\text{Y}_2\text{O}_3$ nanoparticles were synthesized by calcining monodispersed spherical particles of Eu^{3+} -doped yttrium basic carbonate ($\text{Eu}^{3+}:\text{Y}(\text{OH})\text{CO}_3 \cdot n\text{H}_2\text{O}$) grown by homogeneous precipitation (See Ref. [31] for details). The structure and morphology of the nanoparticles were characterized through x-ray diffraction and scanning electron microscopy. In general, the synthesized nanoparticles can be described as nano-ceramics in that each particle consists of an agglomerate of many single nanocrystals as shown in the inset of Fig. 2. The average particle diameter measured by transmission electron microscopy was 400 ± 80 nm, and the average crystallite diameter determined by x-ray diffraction was 130 ± 10 nm. The x-ray diffraction pattern was characteristic of the yttrium oxide body-centered cubic Y_2O_3 structure ($\text{Ia}\bar{3}$ space group) and no evidence of other parasitic phases were found. Furthermore, the line shape and narrow inhomogeneous line width shown in Fig. 2 is consistent with broadening due to isolated Eu^{3+} point defects,^{1,31} which indicates that the concentration of oxygen vacancies and other defects within the crystal structure is low. We note that the nanoparticles studied in this work can be dispersed to be studied individually, which was not the case in previous work where the solvothermal method was used.³⁰ This is an important distinction because individual nanoparticles can be coupled to optical microcavities to fully capitalize on the narrow optical transition line widths obtained in this work.

The homogeneous broadening of the ${}^7\text{F}_0 \leftrightarrow {}^5\text{D}_0$ transition was studied on powdered samples of the nanoparticles to allow the measurement of coherent emission.²⁹ An ensemble can be manipulated to emit coherently using techniques that are the optical equivalents to pulsed spin resonance techniques in the radio frequency and microwave regimes. Specifically, two

coherent pulse sequences were used: two pulse, and three pulse photon echoes. In both techniques the first pulse initializes the ensemble into a superposition of the ground and excited states, the coherence of which decays at a rate governed by the inhomogeneous broadening of the ensemble. In a two pulse echo, the second pulse is an inversion pulse (an optical π pulse in this work), which causes the ensemble to rephase and emit an echo. In contrast, in a three pulse echo, the inversion is divided into two pulses. The second pulse maps the phase evolution to a frequency-dependent population grating, and the third pulse excites this spectral feature resulting in an echo. In these coherent techniques the homogeneous line width is calculated from the decay of the echo as a function of the separation between the first two pulses. In addition to coherent techniques, hole burning measurements were also performed. Hole burning is the use of optical pumping to redistribute ions among the ground state nuclear spin structure of the Eu^{3+} -ions, which results in spectral features with widths governed by the homogenous line width. For details on the experimental method beyond the summary provided in the main text, please refer to the Supporting Information (Section S1) provided.

The powder was maintained at a temperature between 1.3 K and 22.5 K in a liquid helium bath cryostat, using either gas cooling or immersion in liquid helium. The sample holder consisted of a copper plate with a circular aperture (diameter equal to 2 mm and thickness equal to 500 μm), which was filled with the powder and capped on both sides by glass plates. A similar holder made entirely of glass was used for the high magnetic field measurements, which were conducted in a cryostat where both the sample and superconducting coil resided in the helium reservoir. We excited the ${}^7\text{F}_0 \leftrightarrow {}^5\text{D}_0$ transition of the C_2 symmetry Eu^{3+} site within 1 GHz of the central frequency of the inhomogeneously broadened distribution (shown in Fig. 2) at 516.098 THz (580.883 nm in vacuum) using a dye laser with a line width of the order of 300 kHz (Sirah Matisse DS).

The laser was focused onto the powder with a 75 mm focal length lens and the scattered light collected with a 5 mm focal length lens mounted directly behind the sample holder in

the cryostat. For the two pulse and three pulse echo measurements, heterodyne detection was used (see Ref. [30] for details) with large signals observed for a π pulse length of $1.8 \mu\text{s}$ at an input power of 120 mW at the sample (see Supporting Information, Section S2). Although this input power is large compared to single crystal measurements, the scattering effect of the nanoparticles significantly reduces the input power incident on the ions contributing to the coherent signal. For the hole burning measurements, the depleted spectral region (hole) was burned by a 1 ms pulse, and read out by a frequency scan with a duration of $500 \mu\text{s}$. Both the burn and scan had an input power of 12 mW (at the sample) and the hole was detected by monitoring the transmitted intensity of the laser. In all measurements optically pumping all resonant ions to a non-resonant hyperfine ground state was avoided by slowly scanning the laser frequency over a 500 MHz region or by applying a series of chirped pulses between each measurement to return the ensemble to an equilibrium ground state occupancy.

We measured the temperature dependence of the homogeneous line width between 2 and 22.5 K in helium gas using two-pulse photon echoes and hole burning. Both techniques are required because above 6 K the echo amplitude is below the noise level, whereas below 6 K the width of the holes becomes dominated by the laser instability and spectral diffusion. The measured temperature dependence of Γ_h (equal to half the measured hole width) is shown in Fig. 3. This figure also shows the fit of the data according to the model

$$\Gamma_h(T) = \Gamma_0 + \Gamma_l + \alpha_{TLS}T + \alpha_{TPR}T^7 , \quad (1)$$

where Γ_0 is the temperature independent broadening, Γ_l is the broadening contribution of the laser, α_{TLS} describes the coupling of the Eu^{3+} ion to TLS,³² and α_{TPR} describes the rate of TPR interactions.³³ The fitting gives a total value for $\Gamma_0 + \Gamma_l = 370$ kHz, from which we deduce $\Gamma_0 \approx 70$ kHz. The coefficients for the two temperature-dependent terms

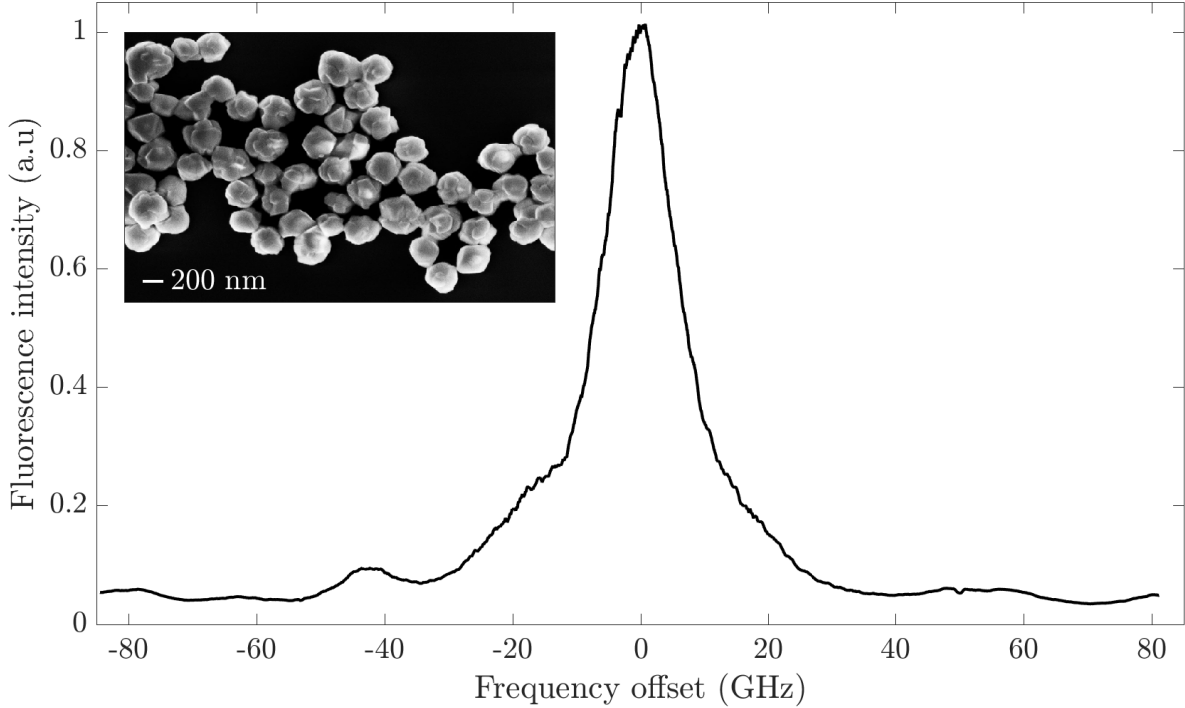


Figure 2: The excitation spectrum of the 0.5% $\text{Eu}^{3+}:\text{Y}_2\text{O}_3$ nanoparticle powder shows the inhomogeneous broadening of the ${}^7\text{F}_0 \leftrightarrow {}^5\text{D}_0$ optical transition. The spectrum was recorded by monitoring the red emission from the optical excited state to the ${}^7\text{F}_2$ crystal field level. The frequency at an offset of 0 was 516.098 ± 0.001 THz. The inset shows a scanning electron microscope image of the studied nanoparticles.

are $\alpha_{TLS} = 4.5 \pm 0.5 \times 10^4$ Hz/K and $\alpha_{TPR} = 5 \pm 1 \times 10^{-3}$ Hz/K⁷, respectively. According to the model, the TLS-interaction dominates the broadening due to phonon interactions for temperatures less than 10 K.

The inset of Fig. 3 shows the results of the two pulse echo study of the temperature dependence below 6 K. In this temperature regime, the broadening due to TPR interactions is negligible, which means that Γ_h can be modeled according to

$$\Gamma_h(T < 6 \text{ K}) = \Gamma_0 + \alpha_{TLS}T \quad . \quad (2)$$

Fitting the photon echo data to Eqn. 2 yielded a TLS coefficient $\alpha_{TLS} = 9 \pm 1 \times 10^3$ Hz/K. This is a more accurate measure of the contribution of the broadening due to TLS because the hole burning data will also contain a contribution due to spectral diffusion on a 250 μs

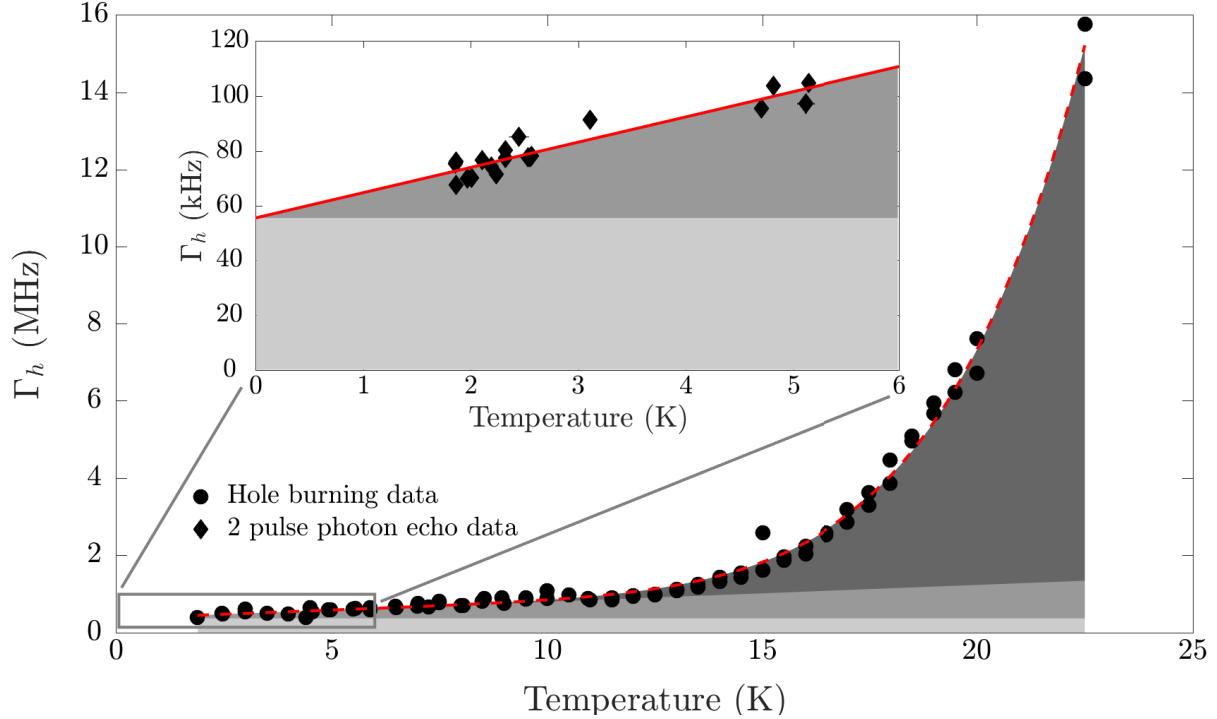


Figure 3: (main figure) The temperature dependence of the homogeneous line width between 2 and 22.5 K measured by hole burning spectroscopy. The fit (dotted line) represents the contributions due to TLS and TPR interactions (see text for details). (inset) Because the hole burning measurement becomes limited by laser instability and spectral diffusion at temperatures below 6 K, two-pulse echoes were used to measure Γ_h at these temperatures. In both the main figure and inset the shaded areas represent the temperature independent broadening (lightest), TLS interaction broadening, and TPR interaction broadening (darkest).

time scale, which will increase more rapidly with temperature compared to the homogeneous broadening.^{34,35}

The photon echo measurements also provide a more accurate value for Γ_0 because the technique is insensitive to the laser line width Γ_l . Extrapolating the data shown in the inset of Fig. 3 to the 0 K limit gives a $\Gamma_0 = 56$ kHz. In the many measurements of $\Gamma_h(T)$ in different regions of the powder the value of Γ_0 showed a variation of the order of 10 kHz despite the fact that α_{TLS} remained constant. For example, the narrowest line width measured to date was 45 ± 1 kHz measured at 1.3 K (see the inset of Fig. 4), which when extrapolated to 0 K gives $\Gamma_0 = 36 \pm 2$ kHz. This variation is attributed to sampling different distributions of nanoparticles in the powder and to temperature differences between the

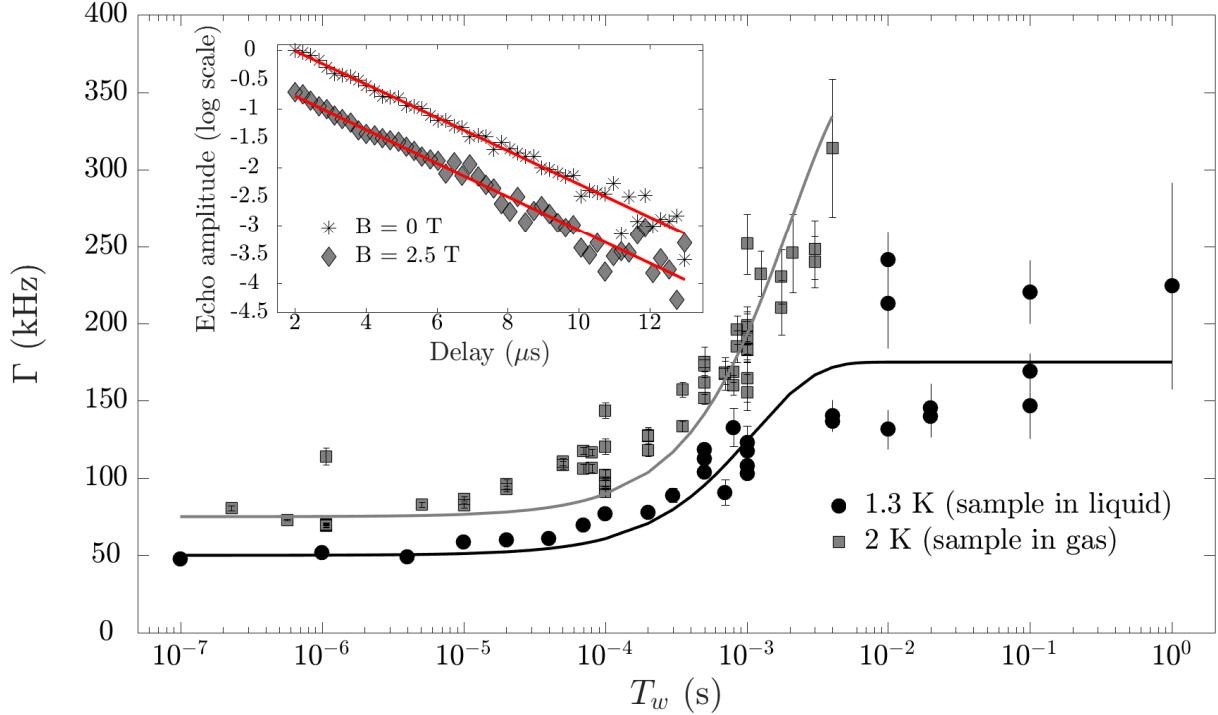


Figure 4: (main figure) 3 pulse photon echo measurements of the spectral diffusion of the optical transition over time scales between 100 ns and 1 s (see text for details). The solid lines are guides to the eye. (inset) Results of two-pulse photon echo measurements at 1.3 K with zero applied field and with an applied field of 2.5 T, respectively. The homogeneous broadening observed in both cases is 45 ± 1 kHz (equivalent to $T_2 = 7.0 \pm 0.2 \mu\text{s}$).

sample and temperature sensor. To reflect this variation the average value of Γ_0 is given as $\overline{\Gamma_0} = 45 \pm 10$ kHz.

In bulk crystals, the temperature independent homogeneous broadening Γ_0 often has a significant contribution from the magnetic field fluctuations due to nuclear or electron spins in the host lattice or impurity spins in lattice defects. This contribution can be reduced by applying static magnetic fields to significantly slow down the rate of spin flips in the lattice. We studied the decay of two-pulse photon echoes in the presence of an applied field ranging from a few mT to 2.5 T. There was no observed variation in Γ_h with magnetic fields applied in this range even at a temperature of 1.3 K (see the inset of Fig. 4).

The spectral diffusion of the europium optical transition in the nanoparticle sample over time is another important parameter for future high spectral resolution applications because

it limits the time scale over which narrow spectral features can be preserved. We studied the broadening of the ion ensemble on time scales between 100 ns and 1 s through three pulse echo studies (see Section S1 in the Supporting Information for details). Fig. 4 shows the results of these measurements at 2 K (cooled by gas) and 1.3 K (cooled by superfluid liquid). Each data point reflects the value of Γ_h obtained by measuring the echo amplitude as the delay τ between the first two pulses was varied for a fixed delay T_w between the second and third pulses. At both temperatures the broadening for $T_w < 100 \mu\text{s}$ is less than 25 kHz. The dominant contribution is likely to be broadening due to TLS interactions, which increases proportional to $\ln(T_w/t_0)$ for t_0 equal to the minimum chosen value of T_w .^{34,35}

When T_w becomes longer than the excited state lifetime $T_1 \approx 1.2 \text{ ms}$,³¹ there is a clear difference in the spectral diffusion at the two temperatures. At 2 K, the broadening increases rapidly for $T_w > T_1$, which prevented measurements on longer time scales because the signal at the shortest achievable delay ($\tau \approx 1 \mu\text{s}$) became indistinguishable from the noise floor. In contrast, at 1.3 K, a sufficiently large signal was observed for $T_w > T_1$ to measure the broadening for time scales up to $T_w = 1 \text{ s}$. An increase in broadening is expected for $T_w > T_1$ in both measurements because relaxation from the excited state back to the initial ground state degrades the spectral grating created by the first two pulses. The spectral grating can also be degraded if the lifetime of the ground state nuclear spin levels T_z is short compared to T_w . Although a change in T_z between 2 K and 1.3 K could be a contributing factor to the observed difference in spectral diffusion behavior, we propose that the dominant mechanism is the long term fluctuations present in our cryostat. Variations in pressure or temperature on a time scale of 1 ms will contribute to the observed broadening. This is because the even distribution of crystalline orientations in the powder means that environmental changes produce a broadening of the ensemble rather than the well defined frequency shift that would be observed in a single crystal. When the sample is immersed under superfluid helium the pressure and temperature stability is greatly improved, which is consistent with the observed results. Although it is not possible to rule out spectral diffusion due to magnetic

perturbations, these interactions are unlikely to be the dominant mechanism. Interactions between Eu^{3+} and nuclear spins are generally much weaker than 200 kHz, whilst electron spins are unlikely to have ms lifetimes at zero field.

At the lower temperature of 1.3 K, the three pulse photon echo can be measured for time scales long compared to T_1 . This is clear evidence that the population grating initially created on the optical transition has been transferred to a population grating between the nuclear spin states through incoherent relaxation. Given that the nuclear spin population grating will relax at a rate of $\exp[-t/T_z]$, it is possible to estimate T_z based on the reduction of the echo amplitude for $T_w > T_1$. If the reduction of the echo amplitude for $\tau = 1 \mu\text{s}$ and $T_w > 4 \text{ ms}$ is attributed entirely to lifetime decay, the exponential fit yields $T_z \approx 450 \text{ ms}$. The spin lifetime and total spectral diffusion observed over 1 s ($< 200 \text{ kHz}$) will both be discussed further in the following section.

The primary aim of this work is to determine the current limit on the optical transition line width, whether there are opportunities for reducing this line width, and what lower bound this fixes for the miniaturization of rare-earth quantum technology hardware. The temperature dependence of Γ_h reveals the dominant broadening mechanisms for temperatures greater than 5 K. Above 15 K, TPR interactions cause the majority of the broadening. In this respect, the observed behavior of the nanoparticles is equivalent to the behavior of europium in bulk crystal samples with the measured value of $\alpha_{TPR} = 5 \pm 1 \times 10^{-3} \text{ Hz/K}^7$ being consistent with measurements in bulk $\text{Eu}^{3+}:\text{Y}_2\text{O}_3$ ($\alpha_{TPR} = 1.4 \times 10^{-3} \text{ Hz/K}^7$ [36]) and bulk $\text{Eu}^{3+}:\text{Y}_2\text{SiO}_5$ ($\alpha_{TPR} = 1.8(7.2) \times 10^{-3} \text{ Hz/K}^7$ for site 1 (site 2)¹). In the temperature range between 5 K and 10 K, the TPR broadening reduces to the extent where interactions between the rare-earth and TLS dominate the homogeneous line width. Although significant TLS interaction broadening is not observed in the highest quality bulk $\text{Eu}^{3+}:\text{Y}_2\text{O}_3$ [28] it has been observed in some bulk $\text{Eu}^{3+}:\text{Y}_2\text{O}_3$ samples, where α_{TLS} can be as high as 18 kHz/K.³⁷ Our previous work on $\text{Eu}^{3+}:\text{Y}_2\text{O}_3$ nanoparticles also reported $\alpha_{TLS} = 18 \text{ kHz/K}$.³⁰ Hence,

the value obtained in this work ($\alpha_{TLS} = 9 \pm 1$ kHz/K) is the lowest value measured in a submicron-diameter particle and within the range observed for bulk crystals.

Importantly, the analysis of the hole burning study enables a bound on the broadening due to the type of size-dependent phonon interactions proposed in Ref. [22]. By fitting the data in Fig. 3 to a model that adds another phonon broadening term βT^3 to Eqn. 1, β is found to be 90 Hz/K³. Thus, the contribution of size-dependent phonon interactions at 1.3 K is less than 200 Hz. This is strong evidence that the mechanism proposed in Ref. [22] is not significantly contributing to the observed line width in our samples. Therefore, the observed relationship between the model proposed in Ref. [22] and the values of Γ_h in nanoparticles with 130 nm diameter crystallites as shown in Fig. 1 is due to another mechanism. Consequently, the observed line width is not necessarily a fundamental limit, allowing the possibility of reducing the line width further. The following analysis characterizes Γ_h to determine what are the contributing interactions and shows that narrower line widths are indeed possible.

Below 3 K, the total broadening due to TLS and TPR interactions are contributing less than 30 kHz of homogeneous broadening. If the homogeneous line width continues to decrease linearly with temperatures below 1.3 K, as is expected for TLS interactions, the extrapolated line width at absolute zero is $\overline{\Gamma}_0 = 45 \pm 10$ kHz. In Eu³⁺-doped bulk crystals the mechanisms that can contribute to Γ_0 can be expressed as

$$\Gamma_0 = \Gamma_{T_1} + \Gamma_{ISD} + \Gamma_{magnetic} \quad , \quad (3)$$

where Γ_{T_1} is the lifetime limited line width, Γ_{ISD} is the broadening due to instantaneous spectral diffusion (ISD) due to dipole-dipole interactions between europium ions,²⁸ and $\Gamma_{magnetic}$ is the broadening due to magnetic fluctuations due to spins in the crystal lattice. Through our measurements we can bound the contributions of the interactions represented in Eqn. 3. The contribution of Γ_{T_1} in these particles is $(2\pi \times 1.2 \text{ ms})^{-1} = 133$ Hz, which is well below the current limit. To investigate the broadening due to ISD the variation of the homoge-

neous line width was measured as a function of the excitation pulse power from 120 mW to ≈ 30 mW (see Section S3 of the Supporting Information). Because Γ_h was insensitive to this variation in excitation power, and hence, the excitation density of Eu^{3+} , we conclude that ISD is not a major broadening interaction. Indeed, from excitation density dependent ISD measurements conducted in bulk $\text{Eu}^{3+}:\text{Y}_2\text{O}_3$ [28] and the excitation bandwidth of the current measurement, we expect Γ_{ISD} to be less than 2 kHz (see Section S3 of the Supporting Information). Finally, it is possible to bound $\Gamma_{magnetic}$ through the results of the photon echo measurements in an applied magnetic field. A field of 2.5 T is sufficient to significantly change the magnetic broadening caused by the flipping of both nuclear and electron spins, yet the homogeneous line width was independent of the applied field. This is strong evidence that magnetic broadening due to lattice or defect-related spins is not the dominant contribution to Γ_h . Given the uncertainty on any one measurement, we can bound the contribution of magnetic broadening to the order of a few kHz.

Therefore, the expected combined broadening in the low temperature limit due to Γ_{T_1} , Γ_{ISD} , and $\Gamma_{magnetic}$ is not more than 5 kHz. In contrast, our measurements indicate that the value for the currently studied nanoparticles is almost an order of magnitude greater than this. Because of the strong evidence that the homogeneous broadening is now dominated by effects other than those observed in bulk crystals it is likely that Γ_h is limited by surface related effects.

Broadening due to fluctuating electric fields at surfaces have previously been studied on spin transitions in nitrogen vacancy centers³⁸ and on optical transitions of quantum dots³⁹ and shown to be a significant source of dephasing. In the following section we analyze the expected broadening due to electric field fluctuations in the europium ion environment arising from charge fluctuations at interfaces between crystallites or the nanoparticle surface. A simple model demonstrates that such an electric field perturbation is sufficient to produce the measured Γ_h and the observed two pulse echo decays are consistent with this mechanism. We model the change in Stark shift experienced by an ensemble of Eu^{3+} ions within a

spherical Y_2O_3 nanoparticle with volume V due to a point charge fluctuation Δq on the surface of the sphere. Because we are studying the system as a powder it is sufficient to consider the charge Δq in an infinite dielectric such that the field at a Eu^{3+} site at a distance r from Δq is

$$\mathbf{E}(r) = \frac{\Delta q}{4\pi\epsilon_0\kappa r^2} \hat{\mathbf{r}} \quad , \quad (4)$$

where ϵ_0 is the vacuum permittivity, and $\kappa = 15$ is the dielectric constant of bulk Y_2O_3 [40].

The Eu^{3+} experiences a linear Stark shift with a Stark coefficient \mathbf{S}

$$\Gamma_{Stark}(r) = \mathbf{S} \cdot \mathbf{E}(r) \quad , \quad (5)$$

but because the crystallites within each nanoparticle are randomly oriented, over the ensemble average it can be assumed that \mathbf{S} and $\mathbf{E}(r)$ are aligned at every point within the sphere. To model the decay of the two pulse echo amplitude as the delay τ between the two pulses is increased we calculate

$$\int_V \exp[-2\pi\tau\Gamma_{Stark}(r)]dV \quad (6)$$

In Fig. 5 the echo amplitude decay over the range of τ used in our experiment is shown for $S = 350 \text{ Hz/ V m}^{-1}$ (the value for site 1 $\text{Eu}^{3+}:\text{Y}_2\text{SiO}_5$ [41]), $|\Delta q| = 1.602 \times 10^{-19} \text{ C}$ (a) and $|\Delta q| = 0.05 \times 1.602 \times 10^{-19} \text{ C}$ (b), and various sphere diameters. The Stark coefficient for $\text{Eu}^{3+}:\text{Y}_2\text{SiO}_5$ is used because it has been well characterized, whereas only an estimate of $S \approx 100 \text{ Hz/ V m}^{-1}$ [42] is published for $\text{Eu}^{3+}:\text{Y}_2\text{O}_3$.

By modeling the system using a single point charge we simulate the maximum possible inhomogeneity of the electric field in the nanoparticle. The result is a broad distribution of line widths, with the maximum broadening for a single electron charge perturbation in

excess of 10 GHz for ions directly adjacent to Δq , > 3 MHz for ions at a distance of 100 nm, and < 250 kHz for ions at a distance of 400 nm. Despite this large inhomogeneity, nearly-exponential two-pulse photon echo decays are predicted for the range of τ accessible in our measurements (see Fig. 5). This is because ions with $\Gamma_h \gg \tau^{-1}$ do not contribute to the coherent signal. Therefore, in the regime where $\Gamma_h > \tau^{-1}$ for all the ions in the nanoparticle, the photon echo inherently selects the ions with the narrowest Γ_h . The predicted line widths are approximately 3.4 MHz, 880 kHz, and 240 kHz for a sphere diameter of 100 nm, 200 nm, and 400 nm, respectively. Given the signal to noise ratio achieved in our experiments, the echo signals shown in part (a) of the figure would only be able to be observed for $\tau < 5 \mu\text{s}$ ($2.2 \mu\text{s}$) for the 400 nm (100 nm) diameter nanoparticles.

Although using Δq equal to a single electron charge provides an easily visualized reference point for comparison, electric field perturbations are more likely to arise from fluctuations in the position and number of multiple surface charges. For a sphere of diameter d and a given surface charge density σ the total number of charges $N = \sigma\pi d^2$ will fluctuate according to Poissonian statistics: $\pm\sqrt{N}$. Because the studied nanoparticles are approximately spherical, that is, their morphology provides symmetry, the average electric field will approach zero for large N . To compare this mechanism to the single electron case, Δq can be scaled to reflect the relative fluctuation \sqrt{N}/N in the electric field. The right hand panel (b) of Fig. 5 shows the photon echo decay curves for Δq a factor of 20 less than a single electron charge, which reflects $N = 400$ or equivalently $\sigma \approx 8 \times 10^{10} \text{ cm}^{-2}$ for a diameter of 400 nm. Single exponential fits to the modeled decays yield additional broadening of approximately 20 kHz (200 kHz) for a sphere of diameter 400 nm (100 nm). Given the calculated σ in other systems,³⁹ it is more likely that the observed broadening is due to charge fluctuations on the surface of the nanoparticle rather than at the interfaces of the contained crystallites. However, the latter cannot be ruled out given the general nature of our model.

Further experiments are needed to confirm that the electric field fluctuation due to surface charges is the dominant broadening mechanisms in our nanoparticles at low temperature.

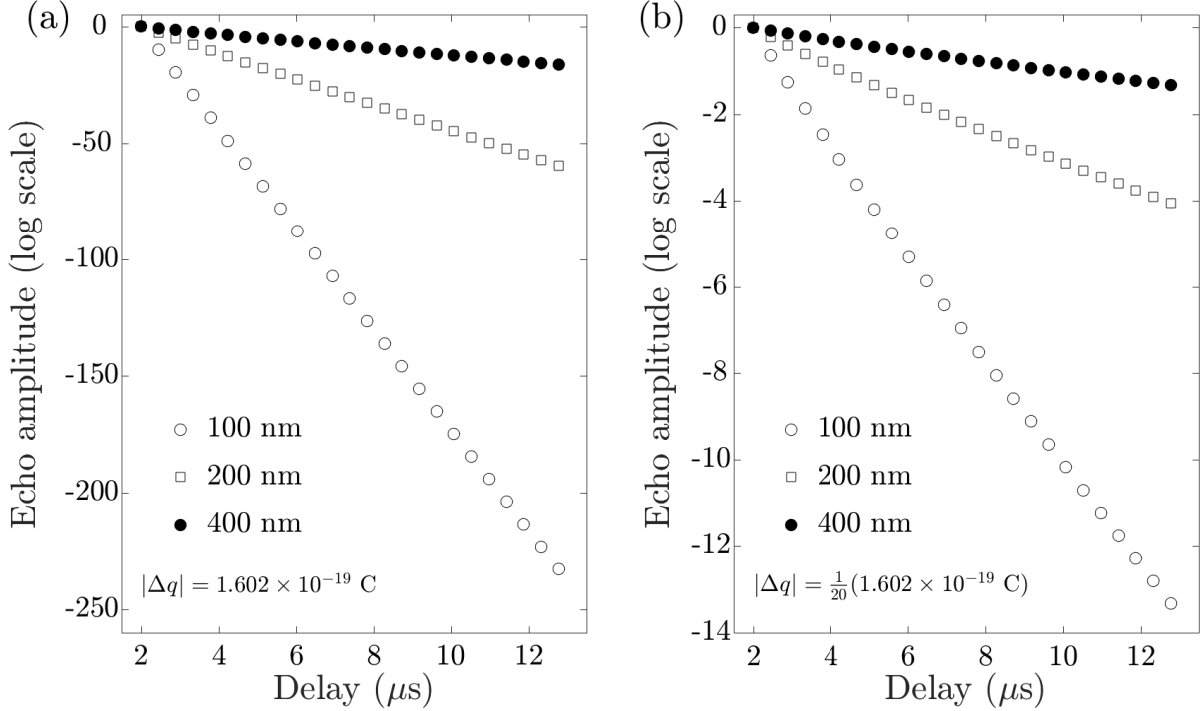


Figure 5: Simulated two-pulse photon echo amplitude decays for $\text{Eu}^{3+}:\text{Y}_2\text{O}_3$ nanoparticles of differing diameter where the only broadening mechanism is that due to a single fluctuating surface charge Δq as described in the text. In (a) Δq is equal to an electron charge, whereas in (b) Δq is reduced by a factor of 20. Even though there is a distribution of homogeneously broadened line widths within each nanoparticle, the echo amplitude decay averaged over the ensemble remains close to exponential. For the case of the smaller Δq , the broadening that produces the echo decay is 200 kHz (100 nm), 60 kHz (200 nm), and 20 kHz (400 nm).

The clearest evidence would be to measure the noise spectrum of the dominant perturbation to confirm that it is consistent with electric field noise. This is possible in the optical domain by employing radiation locking techniques^{43–45} or by performing noise spectrum measurements using optically detected nuclear magnetic resonance techniques³⁸ on the Eu^{3+} spin state transitions.

We now briefly explore to what extent the narrowest observed Γ_h in our system could be reduced under the assumption that the two major broadening interactions at 1.3 K are TLS (≈ 12 kHz) and Stark broadening (≈ 35 kHz). The broadening due to TLS interactions can be reduced by an order of magnitude by cooling the nanoparticles from 1.3 K to the 100 mK operating temperatures possible with dilution fridges. To reduce the remaining Stark

broadening we suggest two strategies. First, using photon echo methods,⁴⁶ it is possible to select ions with the narrowest line widths and shelve ions with broader Γ_h to non-resonant ground state nuclear spin levels. The ‘good’ ions could then be manipulated on a time scale limited by the shelving state lifetime. Second, the nanoparticles could be coated or embedded in a material with a high dielectric constant,³⁸ which would reduce the electric field fluctuations and hence, the broadening. A combination of these techniques should reduce Γ_h to less than 10 kHz for the current nanoparticles.

Although it should be possible to reduce Γ_h to the kHz-level by cooling to 100 mK and employing strategies to reduce Γ_{Stark} , the narrowest line width measured in this work (45 ± 1 kHz) is sufficiently narrow for preliminary investigations of Eu^{3+} - Eu^{3+} electric dipole-dipole interactions. The frequency shift induced by the electric dipole-dipole interaction Δf_{ij} is⁴⁷

$$\Delta f_{ij} = \frac{\mu^2}{4\pi h \epsilon_0 \kappa r_{ij}^3} [\hat{\boldsymbol{\mu}}_i \cdot \hat{\boldsymbol{\mu}}_j - 3(\hat{\boldsymbol{\mu}}_i \cdot \hat{\mathbf{r}}_{ij})(\hat{\boldsymbol{\mu}}_j \cdot \hat{\mathbf{r}}_{ij})] , \quad (7)$$

where μ is the Eu^{3+} electric dipole moment, h is Planck’s constant, and r_{ij} is the separation between ion i and ion j . Based on measured values for μ in other europium crystals,^{41,48} the Δf_{ij} in $\text{Eu}^{3+}:\text{Y}_2\text{O}_3$ should exceed 45 kHz for $r_{ij} < 9$ nm. In comparison, the average separation between Eu^{3+} ions in 0.5% $\text{Eu}^{3+}:\text{Y}_2\text{O}_3$ is approximately 1.3 nm. If Γ_h could be decreased to 5 kHz, $\Delta f_{ij} > \Gamma_h$ for separations up to 20 nm; a volume that would contain approximately 3000 ions.

It is also important to consider how Γ_h scales with the nanoparticle diameter d under the assumption of surface charge fluctuations being the dominant broadening mechanism. The rate at which Γ_{Stark} increases as d is reduced depends on the value of σ . For $\sigma \leq (\pi d^2)^{-1}$, the single surface charge regime, the model derived in this work aptly describes the electric field fluctuations and Γ_{Stark} becomes proportional to d^{-2} . Therefore, in the limit where either σ or d becomes sufficiently small, the model of fluctuating surface charge broadening

would provide a d^{-2} -scaling of the line width with nanocrystal diameter. In contrast, for $\sigma \gg (\pi d^2)^{-1}$, Γ_{Stark} will vary more rapidly as a function of nanocrystal diameter. This is because the strength of the electric field is proportional to d^{-2} and electric field fluctuations due to charges on a spherically symmetric surface are approximately proportional to d^{-1} . This latter regime is most consistent with our experimental results. We note that although attributed to a different interaction, the $d^{-2.5}$ -scaling of the nanocrystal line width observed in Refs. [22,24] lies between the limiting cases discussed above.

If Stark fluctuations on the nanoparticle surface are responsible for the observed Γ_h , by reducing Γ_{Stark} it is feasible to produce isolated 100 nm diameter single crystals with line widths of the order of 10 kHz. Such nanocrystals would be an appealing platform for investigating rare-earth ion quantum information technology in sub-micron scale devices. Contrastingly, without any modification of the Stark broadening interaction, the predicted Γ_h for a 100 nm diameter nanocrystal is of the order of 1 MHz. However, if charge fluctuations at the interface between nanocrystals is the dominant broadening mechanism, the observed Γ_h already reflects the line width for an isolated 100 nm diameter nanocrystal.

The other component of our study was investigating the broadening on longer time scales. The three pulse echo measurements show that spectral diffusion at 1.3 K is less than 100 kHz for time scales less than 1 ms, and less than 200 kHz for time scales up to 1 s. The observed rate of spectral diffusion is at least an order of magnitude less than the rates measured in other disordered systems such as glasses³² and previous studies on $\text{Eu}^{3+}:\text{Y}_2\text{O}_3$ nanoparticles.³⁰ Although low for a disordered material, the rate of spectral diffusion for the nanoparticles studied in this work is large compared to bulk $\text{Eu}^{3+}:\text{Y}_2\text{SiO}_5$, in which no observable spectral diffusion is exhibited on 10 ms time scales.⁴⁹ The likely interactions contributing to the spectral diffusion on short time scales include TLS and Stark broadening. On time scales above 1 ms there will also be a contribution due to pressure and temperature fluctuations in the cryostat.

Importantly, at 1.3 K the spectral diffusion was sufficiently low to observe the decay of

the three pulse echo due to the hyperfine state lifetime $T_z \approx 450$ ms. The measured lifetime is significantly shorter than the value measured in both $\text{Eu}^{3+}:\text{Y}_2\text{O}_3$ bulk crystals ($T_z \approx 80$ h³⁶) and transparent ceramics ($T_z > 30$ min⁵⁰). At this stage it is not possible to identify the mechanism responsible for the reduced T_z but it is likely that a contributing factor is the Eu^{3+} spin flips induced by resonant coupling of magnetic field noise that accompanies the fluctuations in surface charge. Despite the short spin-state lifetime, T_z is long enough to preserve the mapping of a coherent optical state onto the ions' spin state population for up to 1 s. Although further work is required to determine the spin coherence time of the hyperfine transitions, this result opens up interesting opportunities to pursue solid-state quantum optics experiments in a completely new regime. For example, in a regime with 5 kHz optical line widths and spin transitions capable of storing coherence on a 10 ms time scale, it is conceivable to map a photonic quantum state onto the spin states of a known number of nanoparticles and then to change the relative positions of those nanoparticles before the state is retrieved. Such experiments would be able to probe and manipulate spin-wave entangled states in a way not possible in bulk crystals.

In this paper we have performed a thorough spectroscopic analysis of the optical homogeneous line width of europium ions in Y_2O_3 nanoparticles. By studying how the homogeneous line width varied with temperature, magnetic field, and interaction time scale we have characterized the broadening contribution of the known and proposed interactions for rare-earth ion crystals. At high temperature, the broadening is dominated by two phonon Raman processes, completely analogous to bulk crystal systems. For temperatures between 5 and 10 K interactions with TLS cause the majority of the broadening. In the limit of low temperature, these results indicate that size-dependent phonon interactions are not the dominant broadening mechanism for 100 nm crystallites. The remaining 45 ± 10 kHz of broadening is consistent with surface charge fluctuations that create a rapidly varying electric field, which broaden the transition through the linear Stark interaction. Although broadening due to

surface charges has a strong dependence on the size of the nanoparticle, it does not present a fundamental limit to the homogeneous line width. Our study indicates that it is already feasible to resolve ion-ion interaction induced frequency shifts in the measured rare-earth doped nanoparticles. Furthermore, by significantly reducing the effects of surface charge fluctuations and by lowering the temperature below 1 K it should be possible to probe much longer range ion-ion interactions. This result combined with the more complete understanding of the broadening mechanisms gained from this work, and the ability to store coherent states on the longer lived hyperfine transitions, establish an interesting platform for future studies of fundamental and applied quantum mechanics.

Acknowledgement

This project has received funding from the European Union's Seventh Framework Programme FP7/2007-2013/ under REA grant agreement No 287252 (CIPRIS, People Programme-Marie Curie Actions), European Union's Horizon 2020 research and innovation programme under grant agreement No 712721 (NanOQTech) and ANR under grant agreements No 145-CE26-0037-01 (DISCRYS) and 12-BS08-0015-01 (RAMACO).

Supporting Information Available

- Further details on the experiment apparatus and measurement sequences; an estimate of the excitation pulse Rabi frequency; and examples of 2-pulse photon echo decay curves at differing excitation intensities.

This material is available free of charge via the Internet at <http://pubs.acs.org/>.

References

- (1) Könz, F.; Sun, Y.; Thiel, C. W.; Cone, R. L.; Equall, R. W.; Hutcheson, R. L.; Macfarlane, R. M. *Phys. Rev. B* **2003**, *68*, 085109, DOI: 10.1103/PhysRevB.68.085109.
- (2) Zhong, M.; Hedges, M. P.; Ahlefeldt, R. L.; Bartholomew, J. G.; Beavan, S. E.; Wittig, S. M.; Longdell, J. J.; Sellars, M. J. *Nature (London)* **2015**, *517*, 177, DOI: 10.1038/nature14025.
- (3) Hedges, M. P.; Longdell, J. J.; Li, Y.; Sellars, M. J. *Nature (London)* **2010**, *465*, 1052, DOI: 10.1038/nature09081.
- (4) Gündoğan, M.; Ledingham, P. M.; Kutluer, K.; Mazzera, M.; de Riedmatten, H. *Phys. Rev. Lett.* **2015**, *114*, 230501, DOI: 10.1103/PhysRevLett.114.230501.
- (5) Jobez, P.; Laplane, C.; Timoney, N.; Gisin, N.; Ferrier, A.; Goldner, P.; Afzelius, M. *Phys. Rev. Lett.* **2015**, *114*, 230502, DOI: 10.1103/PhysRevLett.114.230502.
- (6) Ledingham, P. M.; Naylor, W. R.; Longdell, J. J. *Phys. Rev. Lett.* **2012**, *109*, 093602, DOI: 10.1103/PhysRevLett.109.093602.
- (7) Wolfowicz, G.; Maier-Flaig, H.; Marino, R.; Ferrier, A.; Vezin, H.; Morton, J. J. L.; Goldner, P. *Phys. Rev. Lett.* **2015**, *114*, 170503, DOI: 10.1103/PhysRevLett.114.170503.
- (8) Fernandez-Gonzalvo, X.; Chen, Y.-H.; Yin, C.; Rogge, S.; Longdell, J. J. *Phys. Rev. A* **2015**, *92*, 062313, DOI: 10.1103/PhysRevA.92.062313.
- (9) Longdell, J. J.; Sellars, M. J. *Phys. Rev. A* **2004**, *69*, 032307, DOI: 10.1103/PhysRevA.69.032307.
- (10) Rippe, L.; Julsgaard, B.; Walther, A.; Ying, Y.; Kröll, S. *Phys. Rev. A* **2008**, *77*, 022307, DOI: 10.1103/PhysRevA.77.022307.

- (11) Utikal, T.; Eichhammer, E.; Petersen, L.; Renn, A.; Götzinger, S.; Sandoghdar, V. *Nat. Commun.* **2014**, *5*, 3627.
- (12) Eichhammer, E.; Utikal, T.; Götzinger, S.; Sandoghdar, V. *New J. Phys.* **2015**, *17*, 083018, DOI: 10.1088/1367-2630/17/8/083018.
- (13) Mader, M.; Reichel, J.; Hänsch, T. W.; Hunger, D. *Nat. Commun.* **2015**, *6*, 7249, DOI: 10.1038/ncomms8249.
- (14) Kelkar, H.; Wang, D.; Martín-Cano, D.; Hoffmann, B.; Christiansen, S.; Götzinger, S.; Sandoghdar, V. *Phys. Rev. Appl.* **2015**, *4*, 054010, DOI: 10.1103/PhysRevApplied.4.054010.
- (15) McAuslan, D. L.; Longdell, J. J.; Sellars, M. J. *Phys. Rev. A* **2009**, *80*, 1–9, DOI: 10.1103/PhysRevA.80.062307.
- (16) Zhong, T.; Kindem, J. M.; Miyazono, E.; Faraon, A. *Nat. Commun.* **2015**, *6*, 8206, DOI: 10.1038/ncomms9206.
- (17) Sinclair, N.; Saglamyurek, E.; George, M.; Ricken, R.; La Mela, C.; Sohler, W.; Tittel, W. *J. Lumin.* **2010**, *130*, 1586–1593, DOI: 10.1016/j.jlumin.2009.12.022.
- (18) Marzban, S.; Bartholomew, J. G.; Madden, S.; Vu, K.; Sellars, M. J. *Phys. Rev. Lett.* **2015**, *115*, 1–5, DOI: 10.1103/PhysRevLett.115.013601.
- (19) Lutz, T.; Veissier, L.; Thiel, C. W.; Woodburn, P. J. T.; Cone, R. L.; Barclay, P. E.; Tittel, W. *Sci. Technol. Adv. Mater.* **2016**, *17*, 63–70, DOI: 10.1080/14686996.2016.1148528.
- (20) Hong, K. S.; Meltzer, R. S.; Bihari, B.; Williams, D. K.; Tissue, B. M. *J. Lumin.* **1998**, *76-77*, 234–237, DOI: 10.1016/S0022-2313(97)89949-8.
- (21) Yang, H. S.; Hong, K. S.; Feofilov, S. P.; Tissue, B. M.; Meltzer, R. S.; Dennis, W. M. *J. Lumin.* **1999**, *84*, 139–145.

- (22) Meltzer, R. S.; Hong, K. S. *Phys. Rev. B* **2000**, *61*, 3396–3403.
- (23) Wakefield, G.; Holland, E.; Dobson, P. J.; Hutchison, J. L. *Adv. Mater.* **2001**, *13*, 1557–1560, DOI: 10.1002/1521-4095(200110)13:20<1557::AID-ADMA1557>3.0.CO;2-W.
- (24) Meltzer, R. S.; Yen, W. M.; Zheng, H.; Feofilov, S. P.; Dejneka, M.; Tissue, B. M.; Yuan, H. B. *Phys. Rev. B* **2001**, *64*, 100201, DOI: 10.1103/PhysRevB.64.100201.
- (25) Mittleman, D. M.; Schoenlein, R. W.; Shiang, J. J.; Colvin, V. L.; Alivisatos, A. P.; Shank, C. V. *Phys. Rev. B* **1994**, *49*, 14435–14447, DOI: 10.1103/PhysRevB.49.14435.
- (26) Takagahara, T. *J. Lumin.* **1996**, *70*, 129–143, DOI: 10.1016/0022-2313(96)00050-6.
- (27) Jobez, P.; Usmani, I.; Timoney, N.; Laplane, C.; Gisin, N.; Afzelius, M. *New J. Phys.* **2014**, *16*, 083005, DOI: 10.1088/1367-2630/16/8/083005.
- (28) Thiel, C. W.; Macfarlane, R. M.; Sun, Y.; Böttger, T.; Sinclair, N.; Tittel, W.; Cone, R. L. Evaluating the practical impact on applications of excitation-induced decoherence in rare-earth-doped optical materials. 2015; Quantum Light-Matter Interaction in Solid State Systems, Barcelona.
- (29) Beaudoux, F.; Ferrier, A.; Guillot-Noël, O.; Chanelière, T.; Le Gouët, J.-L.; Goldner, P. *Opt. Express* **2011**, *19*, 15236, DOI: 10.1364/OE.19.015236.
- (30) Perrot, A.; Goldner, P.; Giaume, D.; Lovrić, M.; Andriamiadamanana, C.; Gonçalves, R. R.; Ferrier, A. *Phys. Rev. Lett.* **2013**, *111*, 203601, DOI: 10.1103/PhysRevLett.111.203601.
- (31) de Oliveira Lima, K.; Gonçalves, R. R.; Giaume, D.; Ferrier, A.; Goldner, P. *J. Lumin.* **2015**, *168*, 276–282, DOI: 10.1016/j.jlumin.2015.08.012.
- (32) Meltzer, R. S. In *Spectroscopic Properties of Rare Earths in Optical Materials*; Liu, G., Jacquier, B., Eds.; Springer Berlin Heidelberg, 2005.

- (33) Orbach, R. *Proc. R. Soc. A* **1961**, *264*, 458–484.
- (34) Black, J. L.; Halperin, B. I. *Phys. Rev. B* **1977**, *16*, 2879–2895, DOI: 10.1103/PhysRevB.16.2879.
- (35) Littau, K. A.; Dugan, M. A.; Chen, S.; Fayer, M. D. *J. Chem. Phys.* **1992**, *96*, 3484–3494, DOI: Doi 10.1063/1.461902.
- (36) Babbitt, W. R.; Lezama, A.; Mossberg, T. W. *Phys. Rev. B* **1989**, *39*, 1987–1992, DOI: 10.1103/PhysRevB.39.1987.
- (37) Flinn, G. P.; Jang, K. W.; Ganem, J.; Jones, M. L.; Meltzer, R. S.; Macfarlane, R. M. *Phys. Rev. B* **1994**, *49*, 5821–5827, DOI: 10.1103/PhysRevB.49.5821.
- (38) Kim, M.; Mamin, H. J.; Sherwood, M. H.; Ohno, K.; Awschalom, D. D.; Rugar, D. *Phys. Rev. Lett.* **2015**, *115*, 087602, DOI: 10.1103/PhysRevLett.115.087602.
- (39) Ha, N.; Mano, T.; Chou, Y.-L.; Wu, Y.-N.; Cheng, S.-J.; Bocquel, J.; Koenraad, P. M.; Ohtake, A.; Sakuma, Y.; Sakoda, K.; Kuroda, T. *Phys. Rev. B* **2015**, *92*, 075306, DOI: 10.1103/PhysRevB.92.075306.
- (40) Robertson, J. *Eur. Phys. J. Appl. Phys.* **2004**, *28*, 265–291, DOI: 10.1051/epjap:2004206.
- (41) Thorpe, M. J.; Leibbrandt, D. R.; Rosenband, T. *New J. Phys.* **2013**, *15*, 033006, DOI: 10.1088/1367-2630/15/3/033006.
- (42) Sun, Y. C. In *Spectroscopic Properties of Rare Earths in Optical Materials*; Liu, G., Jacquier, B., Eds.; Springer Berlin Heidelberg, 2005.
- (43) Sellars, M. J.; Manson, N. B. *J. Lumin.* **1998**, *76 – 77*, 137 – 140, DOI: [http://dx.doi.org/10.1016/S0022-2313\(97\)00194-4](http://dx.doi.org/10.1016/S0022-2313(97)00194-4).

- (44) Pryde, G. J.; Sellars, M. J.; Manson, N. B. *J. Lumin.* **2000**, *86*, 279 – 283, DOI: [http://dx.doi.org/10.1016/S0022-2313\(00\)00189-7](http://dx.doi.org/10.1016/S0022-2313(00)00189-7).
- (45) Pryde, G. J.; Sellars, M. J.; Manson, N. B. *Phys. Rev. B* **2004**, *69*, 075107, DOI: 10.1103/PhysRevB.69.075107.
- (46) Longdell, J. J.; Sellars, M. J.; Manson, N. B. *Phys. Rev. Lett.* **2004**, *93*, 130503, DOI: 10.1103/PhysRevLett.93.130503.
- (47) Van Weperen, W.; Den Hartog, H. W. *Phys. Rev. B* **1978**, *18*, 2857–2865, DOI: 10.1103/PhysRevB.18.2857.
- (48) Ahlefeldt, R. L.; McAuslan, D. L.; Longdell, J. J.; Manson, N. B.; Sellars, M. J. *Phys. Rev. Lett.* **2013**, *111*, 240501, DOI: 10.1103/PhysRevLett.111.240501.
- (49) Yano, R.; Mitsunaga, M.; Uesugi, N. *J. Opt. Soc. Am. B* **1992**, *9*, 992, DOI: 10.1364/JOSAB.9.000992.
- (50) Kunkel, N.; Ferrier, A.; Thiel, C. W.; Ramírez, M. O.; Bausá, L. E.; Cone, R. L.; Ikesue, A.; Goldner, P. *APL Mater.* **2015**, *3*, 1–7, DOI: 10.1063/1.4930221.

Graphical TOC Entry

